EFFECTS OF RADIATION ON MATERIALS

David N. Braski

Vanadium Alloys With Improved Resistance To Helium Embrittlement*

Research metallurgist, Metals & Ceramics Division, Oak Ridge National Laboratory, Oak Ridge, Tennessee 37831-6084

ABSTRACT:

A series of experimental vanadium alloys have been designed with small MC-type carbides in their microstructures to trap helium produced during neutron irradiation, thereby reducing helium embrittlement. The tensile properties and fabricability of the alloys were strongly influenced by the amounts of MC-forming-elements, especially carbon. Alloys with 0.05 and 0.10 wt% carbon exhibited slightly lower yield strengths at 420 to 600°C than vanadium alloys such as V-5Cr-5Ti, Vanstar-7, V-3Ti-1Si, and V-15Cr-5Ti. However, this characteristic may actually be an asset from the standpoint of resistance to irradiation hardening. After implantation with 300 appm ^{3}He, both the V-Ti-C and V-Ti-Zr-C alloys exhibited less ductility losses at 600°C than the other vanadium alloys tested under comparable conditions. Examination of the experimental alloy microstructures by AEM showed that the small MC-type carbides did, in fact, trap helium and that they were responsible for the increased resistance to helium embrittlement of these alloys.

Introduction

Vanadium alloys are being considered for use as a structural first wall of a fusion reactor because they offer a number of advantages over other candidate materials such as stainless steels. These advantages include: low residual activity after irradiation (low activation), high thermal conductivity and low thermal expansion (lower thermal stresses), good mechanical strength at temperature, and good corrosion resistance with a proposed lithium blanket/coolant.[1] However, the vanadium alloys are susceptible to irradiation hardening and helium embrittlement,[2,3] so any improvement in their resistance to these phenomena would increase their viability as a first wall material.

This paper presents the results of a research effort to develop vanadium alloys with improved resistance to helium embrittlement. The approach used to accomplish this goal was to produce a uniform distribution of extremely small carbide particles in the microstructure that will trap helium and reduce embrittlement. Although the trapping of helium at matrix particles may be helpful,[4] the trapping of helium on grain boundary particles is believed to be even more important in reducing helium embrittlement.[5,6] For the trapping to be effective it is important that there be a volumetric misfit between the alloy matrix and the particle. To create the proper particle distributions, it is vital that the carbide particles be dissolved during solution annealing and then reprecipitated during aging at some lower temperature above the service temperature.

This approach has been used for two experimental vanadium alloy types, V-Ti-C and V-Ti-Zr-C. After melting, fabrication, and measurement of tensile properties at temperatures of interest for a fusion reactor first wall,

specimens were implanted with approximately 300 appm of ^{3}He using a modified "tritium trick" procedure[7] and their ductilities were measured to determine the amount of embrittlement. Analytical electron microscopy (AEM) was used in the development of optimum precipitate microstructures and to observe helium trapping. The results of these experiments are presented and discussed herein.

Experimental

The experimental alloys include two different sets, both of which contain fine dispersions of face-centered-cubic (fcc) MC-type carbide particles. The first set includes vanadium with Ti and C additions (alloys V1, V2, V3, V4) that contain MC-type carbide particles. The second set is comprised of alloys with Ti, Zr, and C additions (V7, V8, V10, V11); these alloys contain two MC-type carbides with separate compositions. The composition of each alloy is listed in Table 1. Ingots, weighing 400 g, were arc-cast under argon into water-cooled copper molds. The cast ingots were solution annealed at 1200°C for 1 hr in a vacuum furnace ($p<10^{-4}$ Pa) to dissolve most of the MC particles. The ingots were warm rolled at 500°C from a starting thickness of 1.27 cm down to 0.76 mm with intermediate 30 min.anneals at 1000°C after reaching thicknesses of 0.57 cm and 0.13 cm. Prior to the intermediate anneals and after the final rolling passes, the sheets were pickled in a solution consisting of 6 parts H_2O, 3 parts HNO_3, and 1 part HF (by volume). The sheets were wrapped in Nb-1Zr foil to serve as a getter in the intermediate anneals that were conducted in a vacuum furnace ($p<10^{-3}$ Pa).

Miniature tensile specimens were machined from the 0.76 mm sheet. Disks (3-mm-diam.) for AEM were punched from the sheet and ground down to about 0.3 mm. Tensile specimens and AEM disks from all of the alloys were solution annealed at 1250°C for 1 hr. The specimens in this condition were labeled the solution annealed (SA) condition. Some of the SA specimens of both types were subsequently aged in quartz capsules under 1/2 atm. of argon at 800°C for two weeks; this was called the solution annealed and aged (SA + A) condition. Finally, a third group of as-rolled or 50% warm-worked specimens were also thermally aged using the same parameters to create the warm-worked and aged

(WW + A) condition.

Tensile specimens and AEM disks fabricated from the eight alloys, in all three conditions, were implanted with approximately 300 appm ^{3}He using a modified "tritium trick" technique.[7] Following implantation, specimens with and without helium were tested in tension under vacuum (p<10^{-4} Pa) at 420, 520, and 600°C. AEM disks were dual-jetpolished at -30°C in a solution of 1 part H_2SO_4 and 7 parts methanol (by volume) and then examined in a JEOL 2000FX analytical electron microscope.

Results

Microstructure

The as-cast microstructure for each alloy is shown using optical microscopy in Figs. 1 and 2. The elongated particles in each alloy are carbides. Note that the size and/or number of particles generally increases with carbon content. AEM revealed that many more, even smaller, carbides exist in the as-cast microstructure as shown in Fig. 3. The V-Ti-C alloys, as represented by V1 in Fig. 3a, contains small, thin disks of MC where M is about 25 wt.% V and 75 wt.% Ti. The V-Ti-Zr-C alloys, represented by V7 and V11 (Figs. 3b and 3c), also contain MC, but M is composed of approximately 13.5 wt.% V, 70.9 wt.% Ti, and 15.6 wt.% Zr. A second MC-type carbide was observed in these latter alloys that tended to be blocky with geometric shapes. These particles, which do not appear in the figure, are Zr-rich with M equal to about 1.6 wt% V, 18.3 wt.% Ti, and 80.1 wt.% Zr. It is important to point out that even though the above particles mentioned above are referred to as "carbides," it is very likely that they also contain nitrogen and oxygen. Preliminary electron energy loss spectroscopy (EELS) data showed only

a strong carbon edge for one V-Ti-C alloy that was analyzed, but other data for these alloys would suggest the presence of N and O as well. First, chemical analyses for all of the experimental alloys showed that the N levels were usually at least one-half those of carbon, and that there was always 300 to 500 wt. ppm of oxygen present. Secondly, previous analytical work with vanadium alloys has shown that nitrogen and oxygen are very likely to combine with titanium, vanadium and carbon to form precipitates in vanadium alloys.[8]

Typical microstructures for these three conditions are shown for the V-Ti-C and V-Ti-Zr-C alloys, as represented by V1 and V11, in Figs. 4 and 5, respectively. The microstructures produced by the respective heat treatments in both sets of alloys were found to be quite similar. That is, the SA condition leaves the microstructure with only a few, but sometimes large precipitates (Figs 4a and 5a). Aging at 800°C (SA+A) precipitates thin disks of the Ti-rich MC-type carbides (Figs. 4b and 5b). The disks are parallel to {100} in the crystal and, therefore, have three variants or orientations within each grain. The warm-worked and aged (WW+A) treatment creates a cell structure with many subgrain boundaries and dislocation segments as shown in Figs 4c and 5c. The carbide particles produced by this latter treatment range from 100 to 200 nm in size and have an equiaxed morphology instead of the oriented thin disks found in the SA+A condition.

Fabricability

The relative ease of fabricating each experimental alloy into sheet can be illustrated quite clearly by examination of the final sheets or strips of material that were rolled at 500°C. Fig. 6 is a photograph showing each alloy strip after final rolling to a thickness of 0.76 mm. All of the alloys under

consideration were easily fabricated to the final thickness as evidenced by the relative smooth edges of the strip. However, as more carbon was added, the alloy naturally became stronger and more difficult to roll (compare the strips of V1, V2, and V3 that have increasing amounts of carbon). When an alloy was strengthened too much, as with V9 (V-1.5 wt%Ti-0.15wt%Zr-0.25 wt%C), the strip was literally torn apart by the rolling process.

Tensile Properties

The tensile properties for the eight experimental alloys are listed in Table 2. Looking at the results for V1, it is seen that the SA+A treatment produced a stronger alloy (higher yield strength) with less ductility (total elongation) than the SA condition. The WW+A condition produced even higher yield strengths and lower ductilities than the SA+A. These results are consistent with the observed microstructure for each respective condition (Fig. 4). To elaborate, aging produced large numbers of small carbides that restricted dislocation motion and hardened the material while warm-work produced a similar result by creating dislocation networks. The two effects tended to be additive when the processes were combined. The results are generally the same for the other alloys with minor compositional differences, depending upon the amount of carbon and whether Zr was present. Additional carbon, above the lowest level of 0.05 wt.%, often did not produce alloys that were stronger because the carbide particles were coarse and few in number. Thus, precipitation-hardening effects were minimal. In some cases, the addition of Zr caused additional increases in ultimate strength with little or no corresponding loss in ductility (compare V1-SA with V7-SA, Table 2). In other cases, the alloys with more Zr were slightly weaker and more ductile

(compare V2 with V8). Increasing the amount of Ti from 1.5 to 3.0 wt.%
increased the strength and ductility of V2 to that of V4, but the gain in
strength was lost upon aging. This can be explained by realizing that the
solid solution strengthening offered by the Ti in solution (the SA condition)
was lost when the Ti precipitated out in the Ti-rich MC particles. This left
a weaker matrix with MC particles that were too coarse to cause substantial
precipitation-hardening.

The tensile properties of the V-Ti-C and V-Ti-Zr-C groups as represented
respectively by V1-SA and V11-SA were compared to a group of vanadium alloys
being investigated by the Fusion Materials Program (Fig. 7). The shaded bands
represent the data for V-15Cr-5Ti,[9] Vanstar-7,[9] V-3Ti-1Si,[9] and V-20Ti.[2] The
main conclusion from this comparison is that the experimental vanadium alloys
generally have the same tensile properties as existing vanadium alloys in the
program. One notable exception is the yield strength; the model alloys are
slightly softer than the other vanadium alloys. However, since the ultimate
strengths are not substantially lower, the slightly lower yield strengths may
actually be an advantage with respect to irradiation hardening. With a fairly
large spread between yield and ultimate, the model alloys would be expected to
resist irradiation hardening better than the previous vanadium alloys.

Resistance to Helium Embrittlement

After tensile specimens of each alloy and heat treatment were implanted
with approximately 300 appm ^{3}He, they were tested under the same conditions as
those just described for specimens without helium. The change in ductility
(total elongation) between a specimen that contains helium and a similar one
without helium, is a measure of the alloy's resistance to helium

embrittlement.[7] The ductility changes in the four V-Ti-C and four V-Ti-Zr-C alloys, all in the SA+A condition, are shown for the three test temperatures in Figs. 8 and 9, respectively. All four V-Ti-C alloys actually showed ductility increases at 420°C despite the addition of helium, and exhibited modest losses when the test temperature was increased (Fig. 8). The V-Ti-Zr-C alloys showed similar behavior, with the exception of V7 and V10 which had slight losses at 420°C rather than increases (Fig. 9). This represents a definite improvement in resistance to helium embrittlement relative to any other vanadium alloys that have been tested by the authors under similar conditions. A comparison of V1-SA+A and V11-SA+A with four vanadium alloys tested at 600°C is given in Fig. 10. Both of the experimental vanadium alloys exhibited lower losses in total elongation than any of the other annealed vanadium alloys.[10] In fact, all of the experimental alloys in both the SA+A and WW+A conditions had lower ductility losses than the previous vanadium alloys.

The reason for the improved resistance to helium embrittlement demonstrated by the V-Ti-C and V-Ti-Zr-C alloys is illustrated in Figs. 11 and 12, respectively. The thin Ti-rich MC disks act as sinks for the helium in the microstructure, and helium becomes attached to these particles (Figs. 11a and 12a). This prevents helium from migrating freely to nearby grain boundaries and causing embrittlement. More importantly, Ti-rich MC particles that form within the grain boundaries also trap helium as fine bubbles (Figs. 11b and 12b). The trapping of helium at these two locations enables the alloys to accommodate more helium before serious helium embrittlement occurs. The WW+A condition also is effective in resisting helium embrittlement, but for slightly different reasons. With the warm-worked microstructure, helium

is trapped on dislocations, at subgrain boundaries, and at equiaxed MC
particles, as shown in Figs. 11c and 12c. Furthermore, there appear to be no
high-angle grain boundaries in the WW+A material where helium usually collects
to form the largest bubbles.

Discussion

Previous work using precipitate phases such as carbides in vanadium
alloys has been reported for such alloys as the Vanstar series (using ZrC),
developed by Westinghouse metallurgists,[11] and alloys containing ZrC, ZrN,
various vanadium carbides such as VC and V_2C, developed by the Soviets.[12,13]
In both cases, the particles were utilized for strengthening the alloys and/or
improving the creep properties.

In the present work, it has been demonstrated that the addition of small
amounts of Ti and C or Ti, Zr, and C to pure vanadium will produce a
microstructure with a high number density of small MC-type carbides. The
range of these elements that will produce the desired distributions is fairly
closely represented by the alloys described in Table 1. Carbon less than
approximately 0.05 wt.% will probably result in too few carbides for effective
helium trapping, while amounts of carbon greater than about 0.25 wt.% tend to
produce carbide coarsening and/or agglomeration, which leads to a brittle
alloy.

In small heats cast into water-cooled copper molds, as used in this
study, the carbides precipitate as small thin disks, which would be expected
to serve as excellent traps for helium.[14] Uniform distributions of small MC
particles were also found in the grain boundaries. It was critical that the
carbide particles in both the V-Ti-C and V-Ti-Zr-C alloys could be dissolved

by solution annealing above 1200°C. This will permit the fabricator to first form the material in a "soft" or solution annealed condition and then later precipitate the carbides by aging at somewhat lower temperatures. As in the case of many austenitic stainless steels, this scheme offers opportunities for creating a number of different microstructures by using different aging temperatures, and if desired, aging in combination with cold- or warm- working treatments. The SA + A, and WW + A treatments used in this study demonstrate typical options.

The experimental alloys with the most uniform distributions of carbide particles (see for example V1, V7, and V11 in Figs. 1 &2) had fairly low yield strengths and might be considered too weak for structural applications. However, they also exhibit relatively high values of ultimate strength, suggesting that they may accommodate more irradiation hardening than some of the stronger vanadium alloys, such as Ti-15Cr-5Ti[3], originally developed for nuclear cladding applications. Very little work has been done in measuring the fracture toughness of vanadium alloys, but it would be advantageous to determine this property for the experimental vanadium alloys.

The AEM micrographs show that the carbide particles do, indeed, trap helium, regardless of their location in the microstructure. This effect should extend the lifetime of a nuclear reactor component with regard to helium embrittlement even though such embrittlement appears to be far less a problem than irradiation hardening.[15] The point is that if helium embrittlement can be reduced with no loss in ability to withstand irradiation hardening, the addition of carbide particles would appear to be an advantage. There has been no work on the weldability of these model alloys, but the as-cast microstructures (Fig. 3) are encouraging because they indicate that a

uniform distribution of carbides should form in the fusion zone of the weld.

For these reasons, it appears that adding controlled amounts of carbon and controlling the carbide precipitates in vanadium alloys offer new options for developing vanadium alloys for nuclear applications. With the possible exception of Vanstar-7[11,16], virtually all the vanadium alloys studied under the Fusion Program are alloys in which carbon is never added intentionally. Carbon, as well as other interstitial elements such as nitrogen and oxygen, have been viewed negatively as impurities that generally reduce the ductility of the material. However, this work shows that the addition of small amounts of Zr and/or Ti, effectively tie up the controlled additions of carbon (and probably much of the N and O impurities) to create beneficial precipitate particles. The technique should also provide a basis for developing new structural vanadium alloys with different microstructures and mechanical properties for possible non-nuclear applications.

Conclusions

A series of experimental vanadium alloys have been designed with small MC-type carbides in their microstructures to trap helium produced during neutron irradiation, thereby reducing helium embrittlement. The tensile properties and fabricability of the alloys were strongly influenced by the amounts of MC-forming-elements, especially carbon. Alloys with 0.05 and 0.10 wt% carbon exhibited slightly lower yield strengths at 420 to 600°C than vanadium alloys such as V-5Cr-5Ti, Vanstar-7, V-3Ti-1Si, and V-15Cr-5Ti. However, this characteristic may actually be an asset from the standpoint of resistance to irradiation hardening. After implantation with 300 appm ^{3}He, both the V-Ti-C and V-Ti-Zr-C alloys exhibited less ductility losses at 600°C

than the other vanadium alloys tested under comparable conditions. Examination of the experimental alloy microstructures by AEM showed that the small MC-type carbides did, in fact, trap helium and that they were responsible for the increased resistance to helium embrittlement of these alloys. The idea of adding carbide precipitates to vanadium alloys for resistance to helium embrittlement may offer some new options in developing these alloys for nuclear applications

References

1. D. L. Smith, B. A. Loomis, and D. R. Diercks, "Vanadium-Base Alloys for Fusion Reactor Applications - A Review," Journal of Nuclear Materials, 135, 1985, pp. 125-139.

2. M. P. Tanaka, E. E. Bloom, and J. A. Horak, "Tensile Properties and Microstructure of Helium Injected and Reactor Irradiated V-20Ti," Journal of Nuclear Materials, 103&104, 1981, pp. 895-900.

3. D. N. Braski, "The Effect of Neutron Irradiation on the Tensile Properties and Microstructure of Several Vanadium Alloys," Influence of Radiation on Material Properties: 13th Intern. Symposium (part II), ASTM STP 956, F. A. Garner, C. H. Henager, Jr., and N. Igata, Eds., American Society for Testing and Materials, Philadelphia, 1987, pp. 271-290.

4. W. Kesternich, "A possible Solution of the Problem of Helium Embrittlement," Journal of Nuclear Materials, 127, 1985, pp. 153-160.

5. A. F. Rowcliffe, G. J. C. Carpenter, H. F. Merrick, and R. B. Nicholson, "An Electron Microscope Investigation of High-Temperature Embrittlement of Irradiated Stainless Steels," Effects of Radiation on Structural Metals, American Society for Testing and Materials, ASTM STP 426, Philadelphia, 1967, pp. 161-199.

6. P. J. Maziasz and D. N. Braski, "Microstructural Design of PCA Austenitic Stainless Steel for Improved Resistance to Helium Embrittlement Under HFIR Irradiation," Journal of Nuclear Materials, 122&123, 1984, pp. 305-310.

7. D. N. Braski and D. W. Ramey, "A Modified Tritium Trick Technique for Doping Vanadium Alloys with Helium," Effects of Radiation on Materials: 12th Intern. Symposium, ASTM STP 870, F. A. Garner and J. S. Perrin, Eds., American Society for Testing and Materials, Philadelphia, 1985, pp. 1211-1224.

8. T. Schober and D. N. Braski, "The Microstructure of Selected Annealed Vanadium-Base Alloys," Metallurgical Transactions A, Vol. 20A, Oct. 1989, pp. 1927-1932.

9. D. N. Braski, "The Tensile Properties and Swelling of Several Vanadium Alloys After Irradiation to 40 dpa in FFTF," Alloy Development for Irradiation Performance - Semiannual Progress Report, March 31, 1986, DOE/ER-0045/16, p. 61.

10. D. N. Braski, unpublished data.

11. G. A. Whitlow, R. A. Nadler, and R. C. Svedberg, "Vanadium Alloy Cladding Development - Final Report," Westinghouse Advanced Reactors Division Report, WARD-3791-47, November 1970.

12. E. M. Lyutyi and V. V. Shirokov, "Influence of Long High-Temperature Aging in Vacuum on the Strength Properties of Vanadium Alloys," Fiziko-Khimicheskaya Mekhanika Materialov, Vol. 16, No. 3, May-June 1980, pp. 53-56.

13. O. I. Bankovskii, O. M. Barabash, and V. I. Kornilova, "Comparative Characteristics of Dispersion Hardening of Vanadium by Zirconium Carbide and Nitride," Izvestiya Akademii Nauk SSSR, Metally, Vol. 1, 1985, pp. 143-147.

14. D. N. Braski, "Doping of Vanadium Alloys with Helium Using Tritium," Proceedings of the 45th Annual Meeting of the Electron Microscopy Society of America, G. W. Bailey, Ed., San Francisco Press, Inc., San Francisco, 1987, pp. 218-219.

15. D. N. Braski, "The Postirradiation Tensile Properties and Microstructure of Several Vanadium Alloys," Symposium on Reduced Activation Materials for Fusion Reactors, ASTM STP 1047, R. L. Klueh, D. S. Gelles, M. Okada, and N. H. Packan, Eds., American Society for Testing and Materials, Philadelphia, 1989, pp. 161-178.

16. W. Pollack, R. W. Buckman, R. T. Begley, K. C. Thomas, and E. C. Bishop, "Development of High Strength Vanadium Alloys - Final Report," AEC Research and Development Report UC 25, Westinghouse Electric Corp., June 1967.

Figure Captions

Fig. 1 - Light micrographs showing the as-cast microstructure of V-Ti-C
alloys: (a) V1, (b) V2, (c) V3, and (d) V4.

Fig. 2 - Light micrographs showing the as-cast microstructure of V-Ti-Zr-C
alloys: (a) V7, (b) V8, (c) V10, and (d) V11.

Fig. 3 - Transmission electron micrographs showing the detailed as-cast
microstructure of alloys: (a) V1, (b) V7, and (c) V11.

Fig. 4 - Microstructure of V1 alloy in the (a) solution annealed
1 h at 1250°C (SA), (b) solution annealed 1 h at 1250°C and aged
2 wks. at 800°C (SA+A), and (c) 50% warm-worked and aged 2 wks.
at   800°C (WW+A), conditions.

Fig. 5 - Microstructure of V11 alloy in the (a) solution annealed 1 hr at
1250°C (SA), (b) solution annealed 1 hr at 1250°C and aged 2 wks. at
800°C (SA+A), and (c) 50% warm-worked and aged 2 wks at 800°C (WW+A),
conditions.

Fig. 6 - Warm-rolled sheets of advanced vanadium alloys.
Thickness of sheets = 0.76 mm.

Fig. 7 - Tensile properties of V1-SA and V11-SA compared to the band of properties representing V-15Cr-5Ti (ref. 9), Vanstar-7 (ref. 9), V-3Ti-1Si (ref. 9), and V-20Ti (ref. 2).

Fig. 8 - The ductility changes in V-Ti-C alloys due to 300 appm implanted helium.

Fig. 9 - The ductility changes in V-Ti-Zr-C alloys due to 300 appm implanted helium.

Fig. 10 - Ductility losses in vanadium alloys at 600°C due to 300 appm implanted helium.

Fig. 11 - Microstructure of (a) V1-SA+A matrix, (b) V1-SA+A grain boundary, and (c) V1-WW+A matrix after implantation of 300 appm [3]He showing how the helium is trapped at Ti-rich MC particles (a, b, and c) and subgrain boundaries (c).

Fig. 12 - Microstructure of (a) V11-SA+A matrix, (b) V11-SA+A grain boundary, and (c) V11-WW+A matrix after implantation of 300 appm [3]He showing how the helium is trapped at Ti-rich MC particles (a, b, and c) and subgrain boundaries (c).

Table 1. Vanadium alloy composition

Alloy No.	Composition, wt %			
	V	Ti	Zr	C
V1	98.45	1.5		0.05
V2	98.40	1.5		0.10
V3	98.25	1.5		0.25
V4	96.90	3.0		0.10
V7	98.30	1.5	0.15	0.05
V8	98.25	1.5	0.15	0.10
V10	96.75	3.0	0.15	0.10
V11	98.10	1.5	0.30	0.10

Table 2. Tensile properties

Alloy	Specimen No.	Condition	Test Temperature (°C)	Stress, MPa		Elongation, %	
				Yield	Ultimate	Uniform	Total
V1	V107	SA[a]	420	266	438	11.2	17.0
V1	V108	SA	520	255	515	18.1	22.8
V1	V104	SA	600	256	524	16.6	22.3
V1	V111	SA + A[b]	420	313	424	8.0	13.3
V1	V113	SA + A	520	327	438	7.3	14.7
V1	V121	SA + A	600	312	429	8.7	16.7
V1	V103	WW + A[c]	420	353	412	5.7	13.3
V1	V106	WW + A	520	356	424	6.3	14.7
V1	V118	WW + A	600	366	429	5.3	13.0
V2	V202	SA	420	242	521	14.8	20.6
V2	V215	SA	520	240	442	10.8	15.6
V2	V217	SA	600	251	582	18.3	22.6
V2	V219	SA + A	420	325	475	8.3	15.0
V2	V223	SA + A	520	346	492	8.7	16.0
V2	V224	SA + A	600	331	463	8.7	16.7
V2	V204	WW + A	420	369	415	6.0	14.0
V2	V212	WW + A	520	369	440	6.7	16.7
V2	V221	WW + A	600	383	457	6.7	14.3
V3	V309	SA	420	237	424	10.8	16.2
V3	V317	SA	520	237	538	14.8	21.0
V3	V313	SA	600	237	570	20.0	30.5
V3	V307	SA + A	420	293	482	9.0	14.3
V3	V304	SA + A	520	336	589	11.7	16.3
V3	V315	SA + A	600	308	578	12.3	25.0
V3	V302	WW + A	420	461	586	9.7	13.3
V3	V305	WW + A	520	475	593	9.7	13.0
V3	V321	WW + A	600	458	593	8.7	21.7
V4	V410	SA	420	324	404	13.8	22.3
V4	V418	SA	520	284	551	19.6	27.0
V4	V420	SA	600	281	571	20.3	28.0
V4	V402	SA + A	420	219	376	11.0	18.7
V4	V411	SA + A	520	221	391	11.6	19.5
V4	V421	SA + A	600	224	388	14.2	19.0
V4	V405	WW + A	420	293	376	8.3	15.9
V4	V407	WW + A	520	280	372	9.1	16.8
V4	V412	WW + A	600	296	393	7.5	13.8

Table 2 (contd.)

Alloy	Specimen No.	Condition	Test Temperature (°C)	Stress, MPa		Elongation, %	
				Yield	Ultimate	Uniform	Total
V7	V713	SA	420	246	414	12.2	20.5
V7	V714	SA	520	240	520	15.9	22.0
V7	V721	SA	600	244	567	15.8	21.6
V7	V703	SA + A	420	250	394	10.3	19.0
V7	V704	SA + A	520	263	416	10.3	18.0
V7	V706	SA + A	600	253	406	11.0	16.7
V7	V702	WW + A	420	335	394	6.7	15.0
V7	V705	WW + A	520	339	409	7.0	14.0
V7	V722	WW + A	600	342	407	7.3	12.7
V8	V801	SA	420	226	494	13.8	18.8
V8	V804	SA	520	207	518	15.5	20.9
V8	V817	SA	600	228	569	20.6	27.6
V8	V802	SA + A	420	220	402	10.0	16.0
V8	V809	SA + A	520	240	420	10.3	17.3
V8	V818	SA + A	600	234	431	12.7	21.7
V8	V811	WW + A	420	349	419	7.0	14.3
V8	V820	WW + A	520	362	432	6.7	12.3
V8	V821	WW + A	600	374	446	7.0	15.0
V10	V1001	SA	420	245	432	13.2	22.4
V10	V1019	SA	520	246	533	15.5	23.0
V10	V1015	SA	600	237	511	16.2	25.4
V10	V1003	SA + A	420	199	344	11.7	21.0
V10	V1007	SA + A	520	188	350	12.3	20.0
V10	V1008	SA + A	600	201	357	11.3	19.7
V10	V1010	WW + A	420	296	381	8.0	15.7
V10	V1011	WW + A	520	293	372	8.7	16.0
V10	V1013	WW + A	600	305	376	7.3	13.7
V11	V1123	SA	420	244	433	14.0	22.5
V11	V1105	SA	520	254	558	15.0	20.6
V11	V1119	SA	600	247	568	19.4	26.2
V11	V1110	SA + A	420	317	456	8.9	17.0
V11	V1122	SA + A	520	324	466	8.0	16.0
V11	V1124	SA + A	600	319	472	9.3	17.7
V11	V1104	WW + A	420	388	456	5.7	11.3
V11	V1108	WW + A	520	408	483	5.7	11.7
V11	V1113	WW + A	600	403	469	5.7	12.0

[a]SA = solution annealed 1 h at 1250°C.

[b]SA + A = solution annealed 1 h at 1250°C and aged two weeks at 800°C.

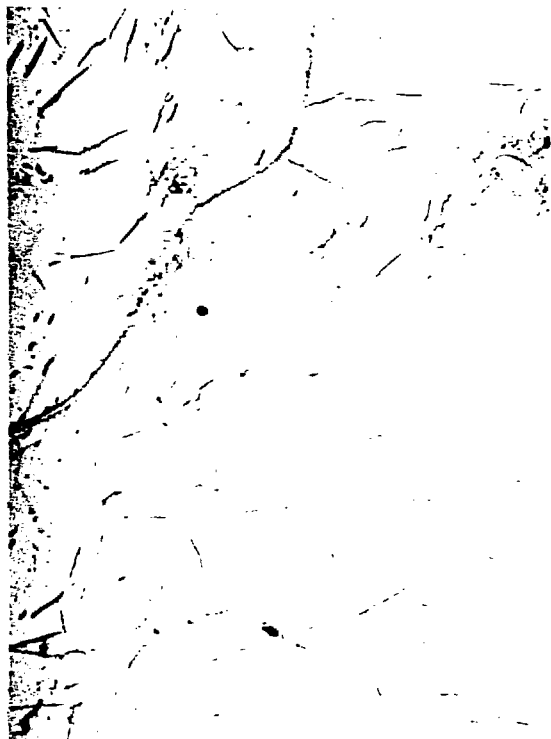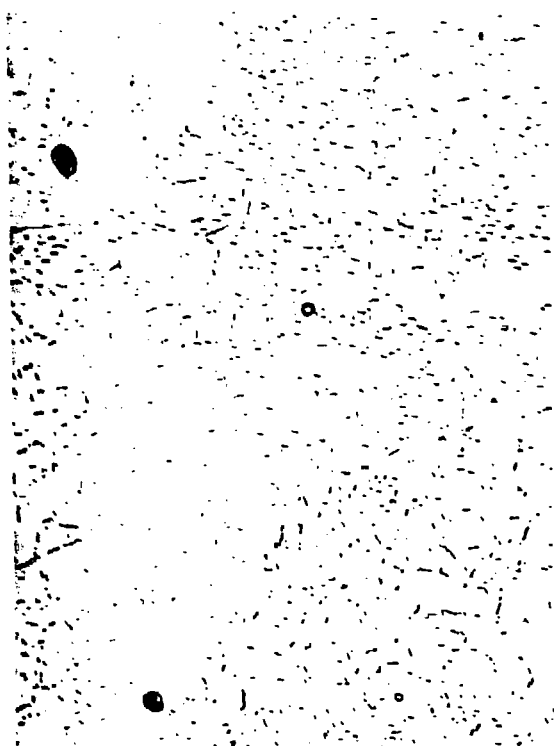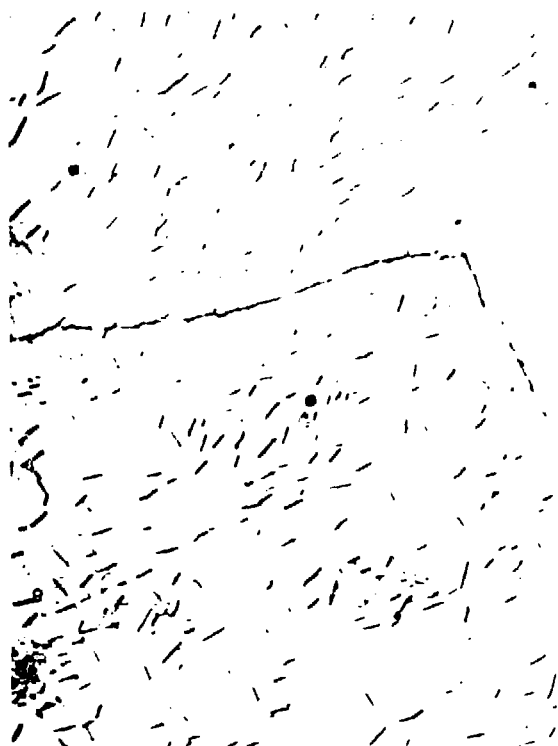[c]WW + A = 50% warm worked and aged two weeks at 800°C.
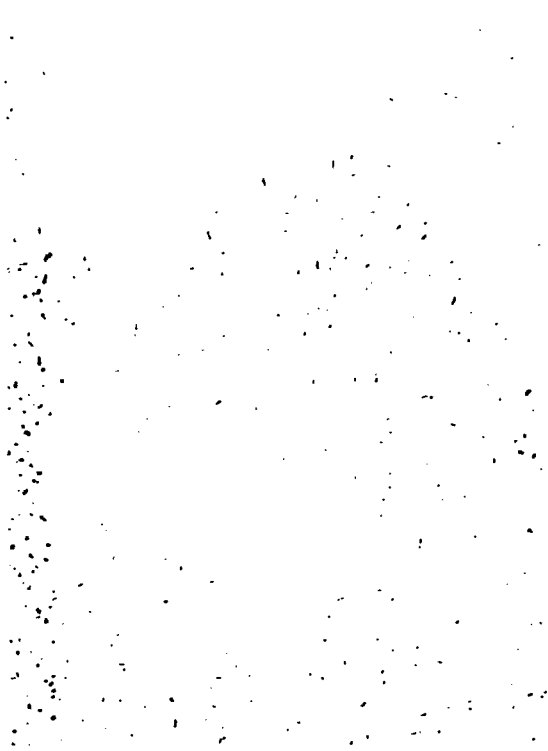
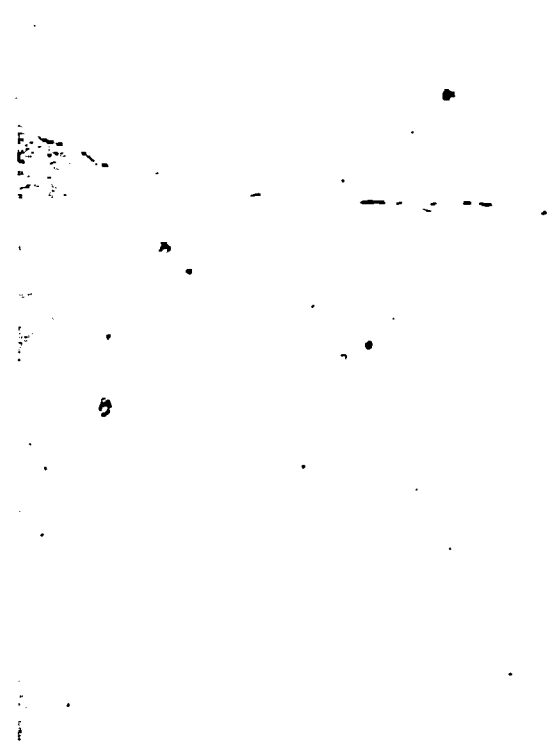(a)　　　　　　　　　　　　　　　　(b)

(c)　　　　　　10 μm　　　　　(d)

Fig. 1 - Light micrographs showing the as-cast micro-
structure of V-Ti-C alloys: (a) V1, (b) V2,
(c) V3, and (d) V4.

(a)

(b)

(c)

10 μm

(d)

Fig. 2 - Light micrographs showing the as-cast micro-
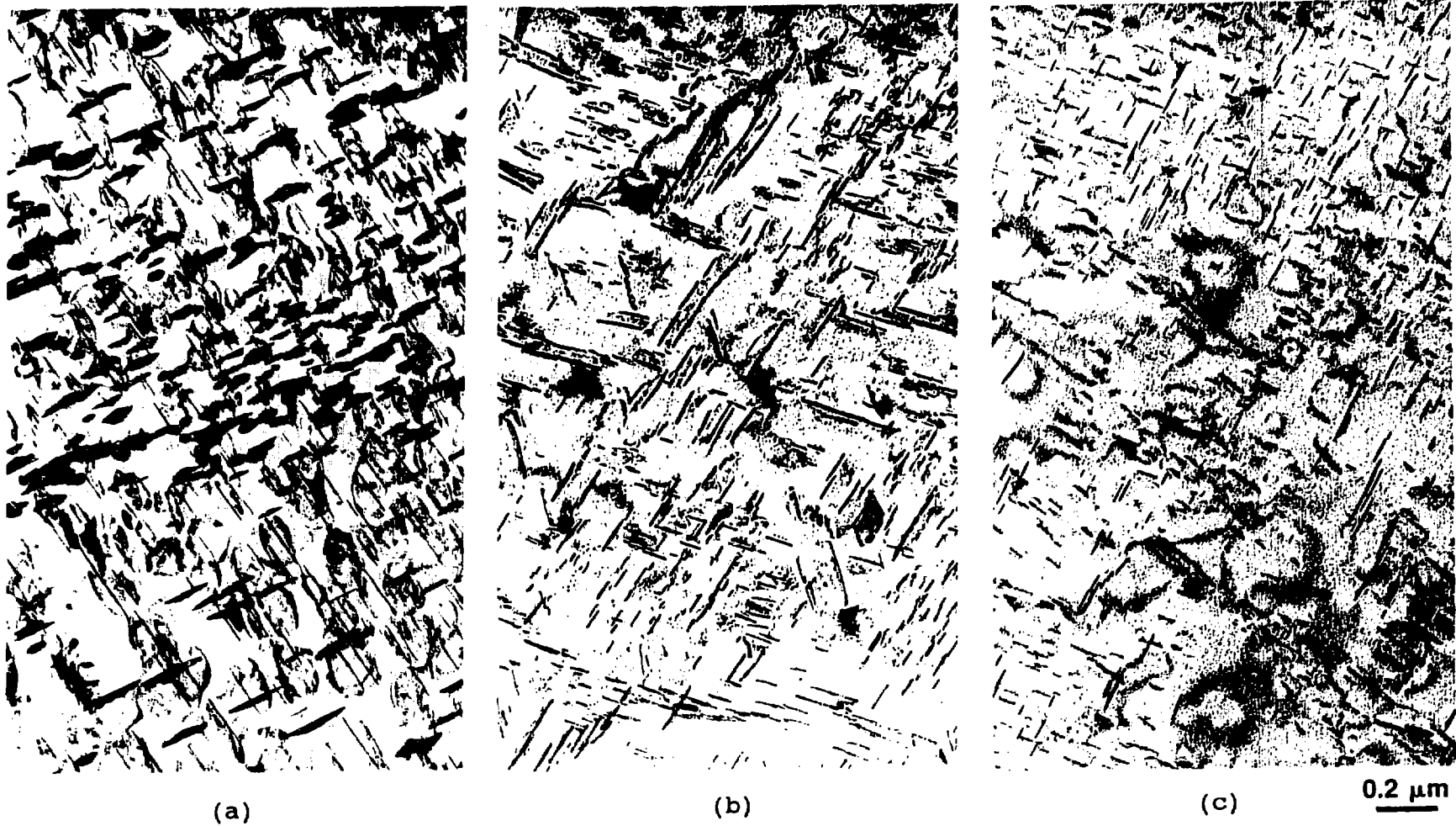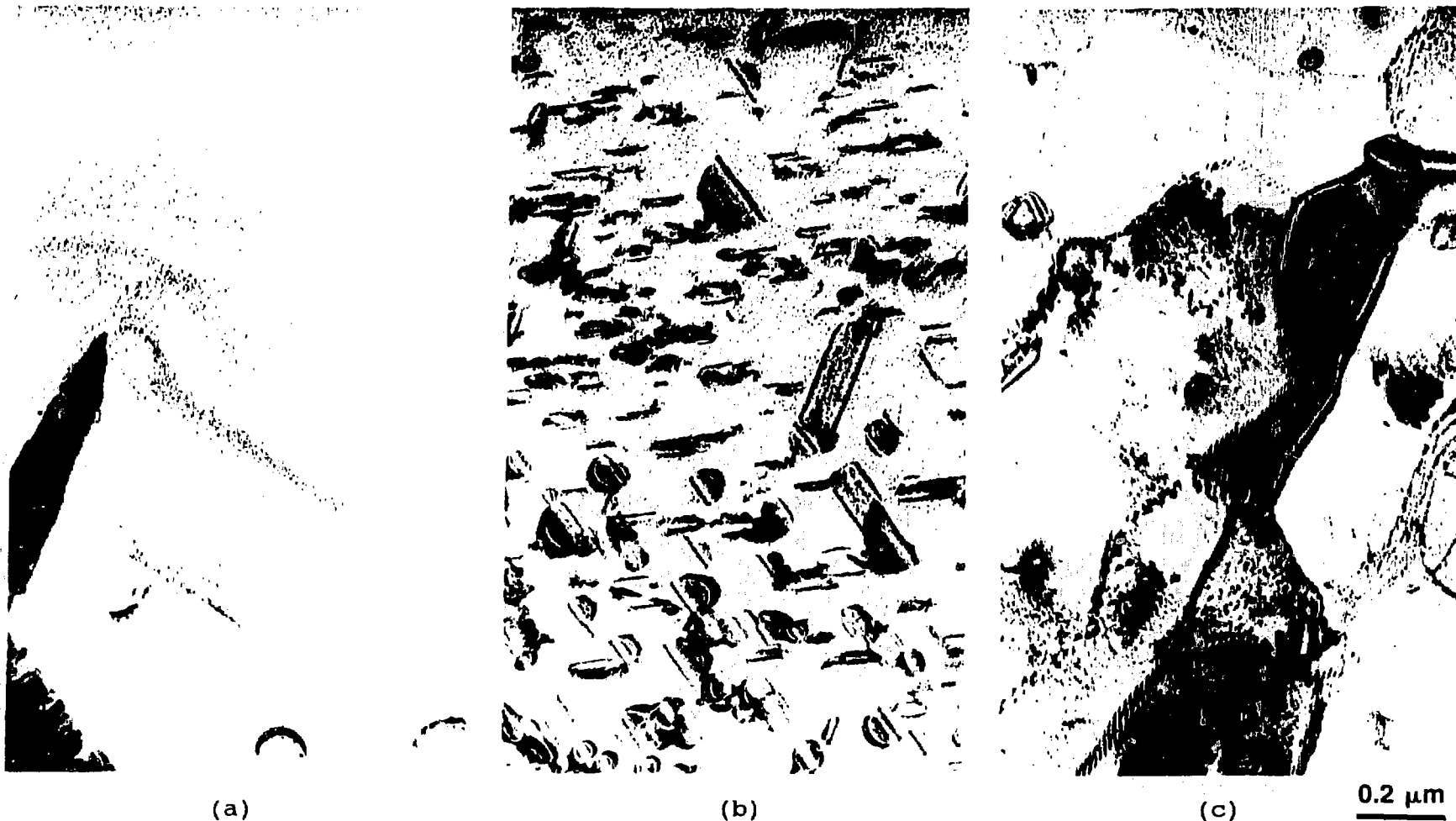structure of V-Ti-Zr-C alloys: (a) V7, (b) V8,
(c) V10, and (d) V11.

0.2 μm

Fig. 3 – Transmission electron micrographs showing the
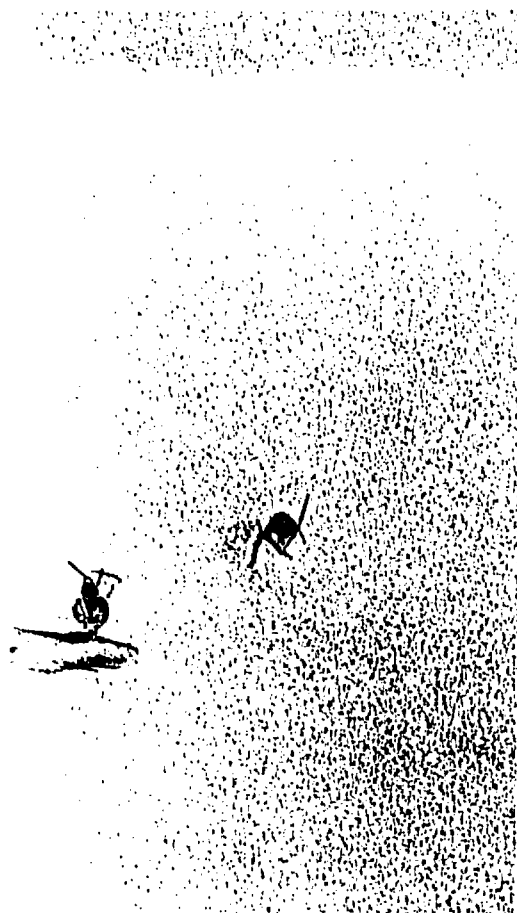detailed as-cast microstructure of alloys: (a) V1,
(b) V7, and (c) V11.

(a)   (b)   (c)   0.2 μm

Fig. 4 - Microstructure of V1 alloy in the (a) solution
         annealed 1 h at 1250°C (SA), (b) solution
         annealed 1 h at 1250°C and aged 2 wks. at 800°C
         (SA+A), and (c) 50% warm-worked and aged 2 wks.
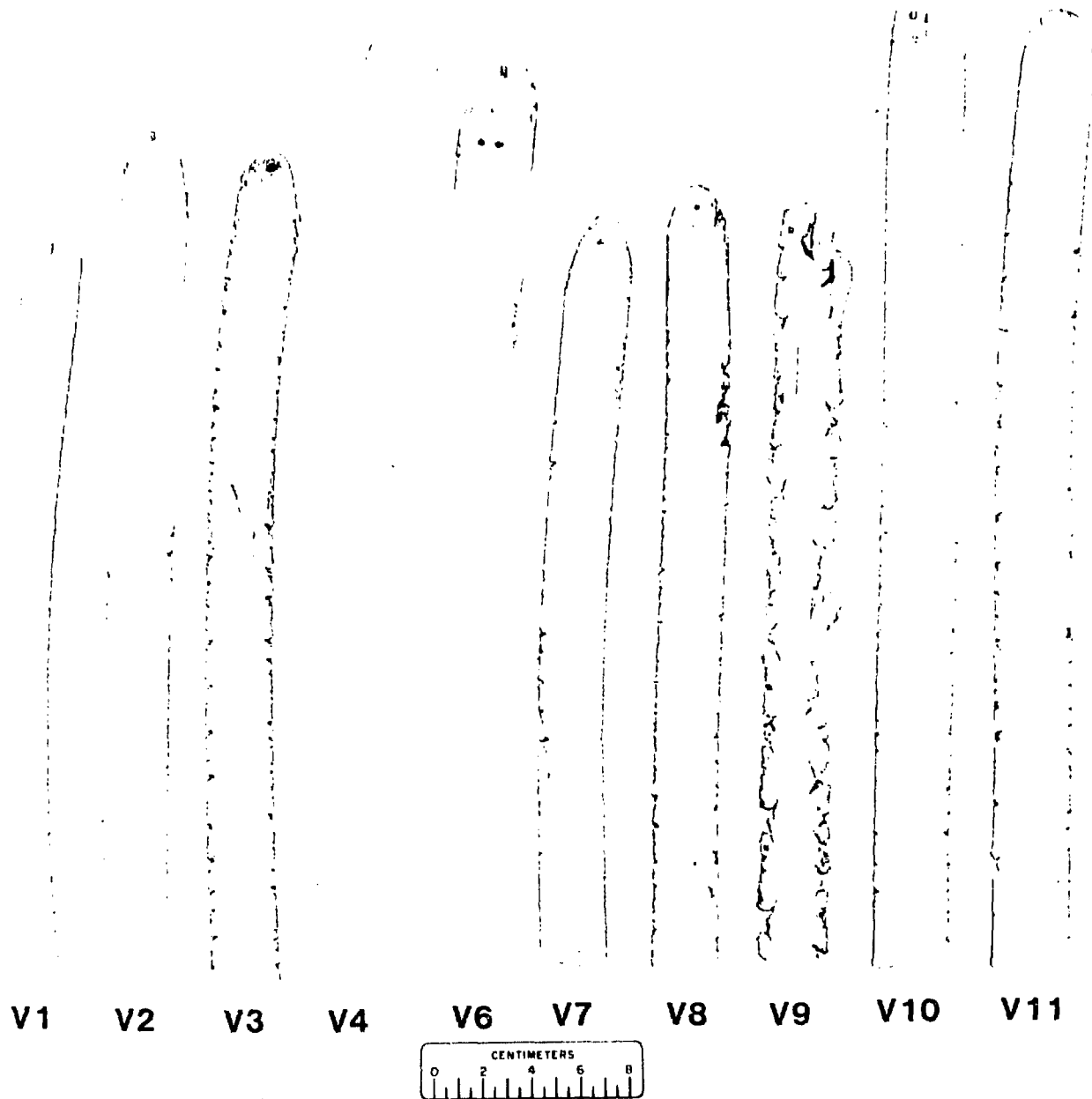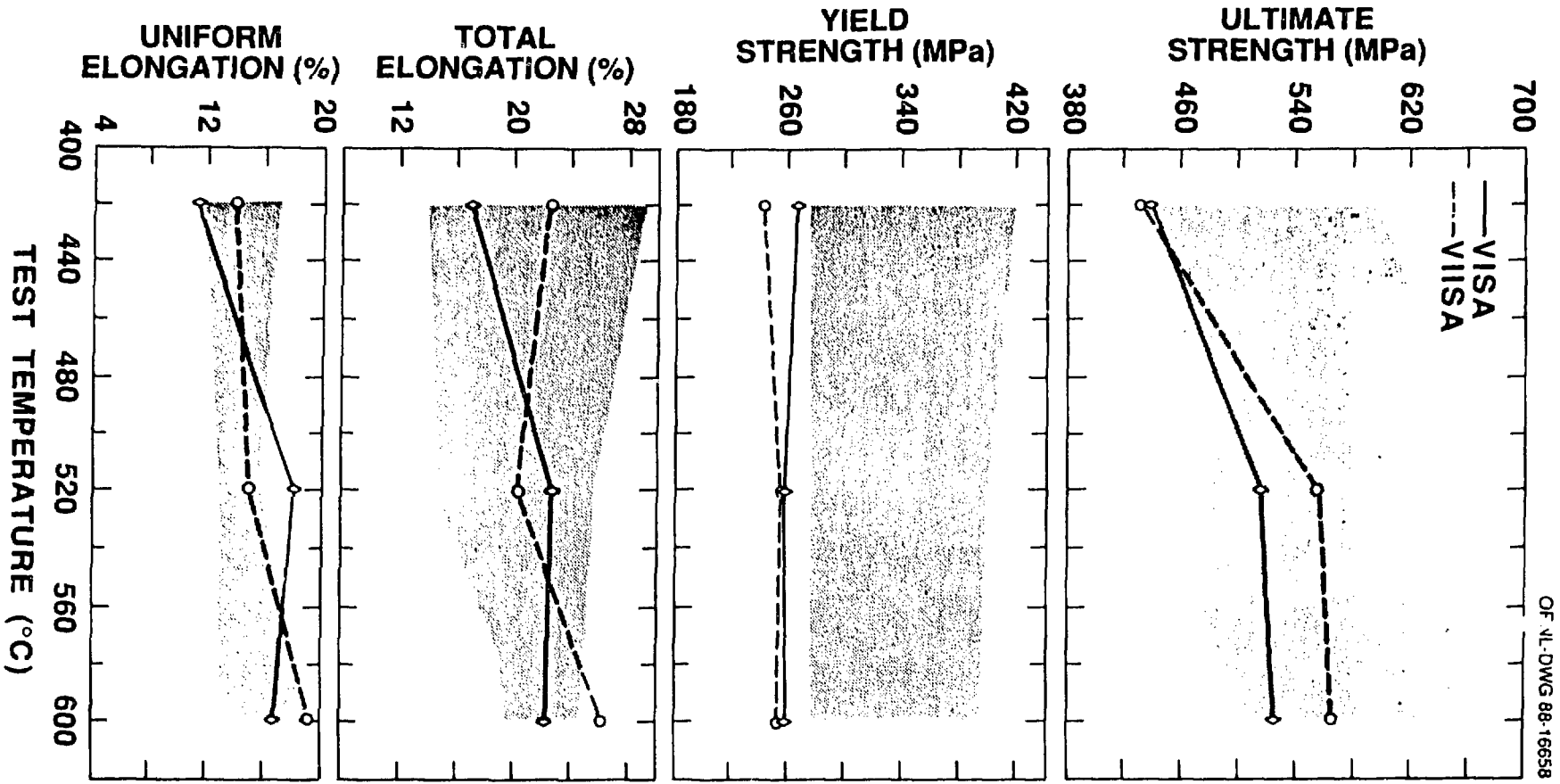   at 800°C (WW+A), conditions.

Fig. 5 - Microstructure of V11 alloy in the (a) solution
annealed 1 hr at 1250°C (SA), (b) solution
annealed 1 hr at 1250°C and aged 2 wks. at 800°C
(SA+A), and (c) 50% warm-worked and aged 2 wks.
at 800°C (WW+A), conditions.

V1   V2   V3   V4   V6   V7   V8   V9   V10   V11

CENTIMETERS
0   2   4   6   8

Fig. 6 - Warm-rolled sheets of advanced vanadium alloys.
Thickness of sheets = 0.76 mm.

UNIFORM ELONGATION (%)

TOTAL ELONGATION (%)

YIELD STRENGTH (MPa)

ULTIMATE STRENGTH (MPa)

TEST TEMPERATURE (°C)

V1SA
V11SA

OF VL-DWG 88-16658

Fig. 7 – Tensile properties of V1-SA and V11-SA compared to band of properties representing 2 heats of V-15Cr-5Ti, Vanstar-7, V-3Ti-1Si, and V-20Ti.

Fig. 8 –

Ductility Changes in V-Ti-C Alloys Due to 300 appm Implanted Helium
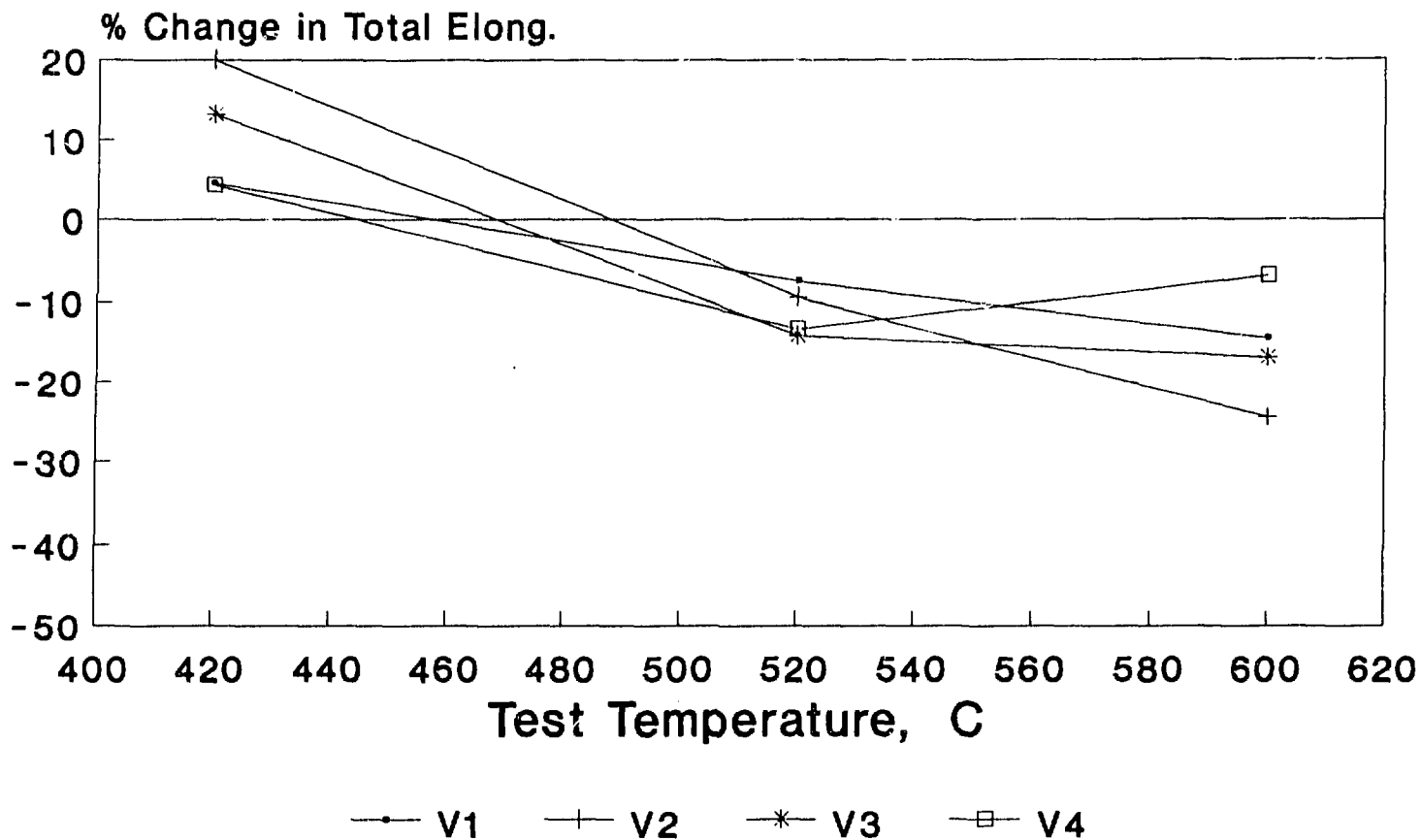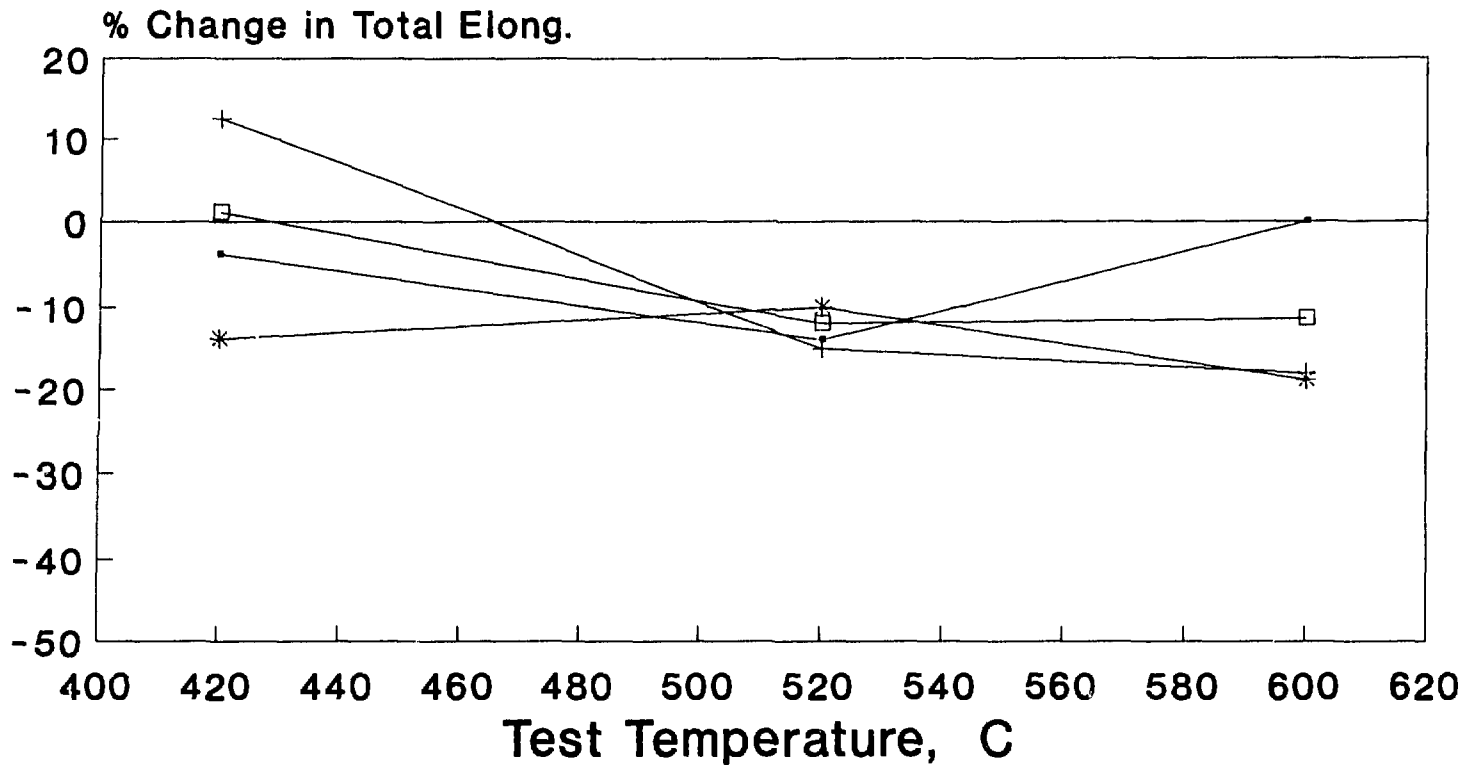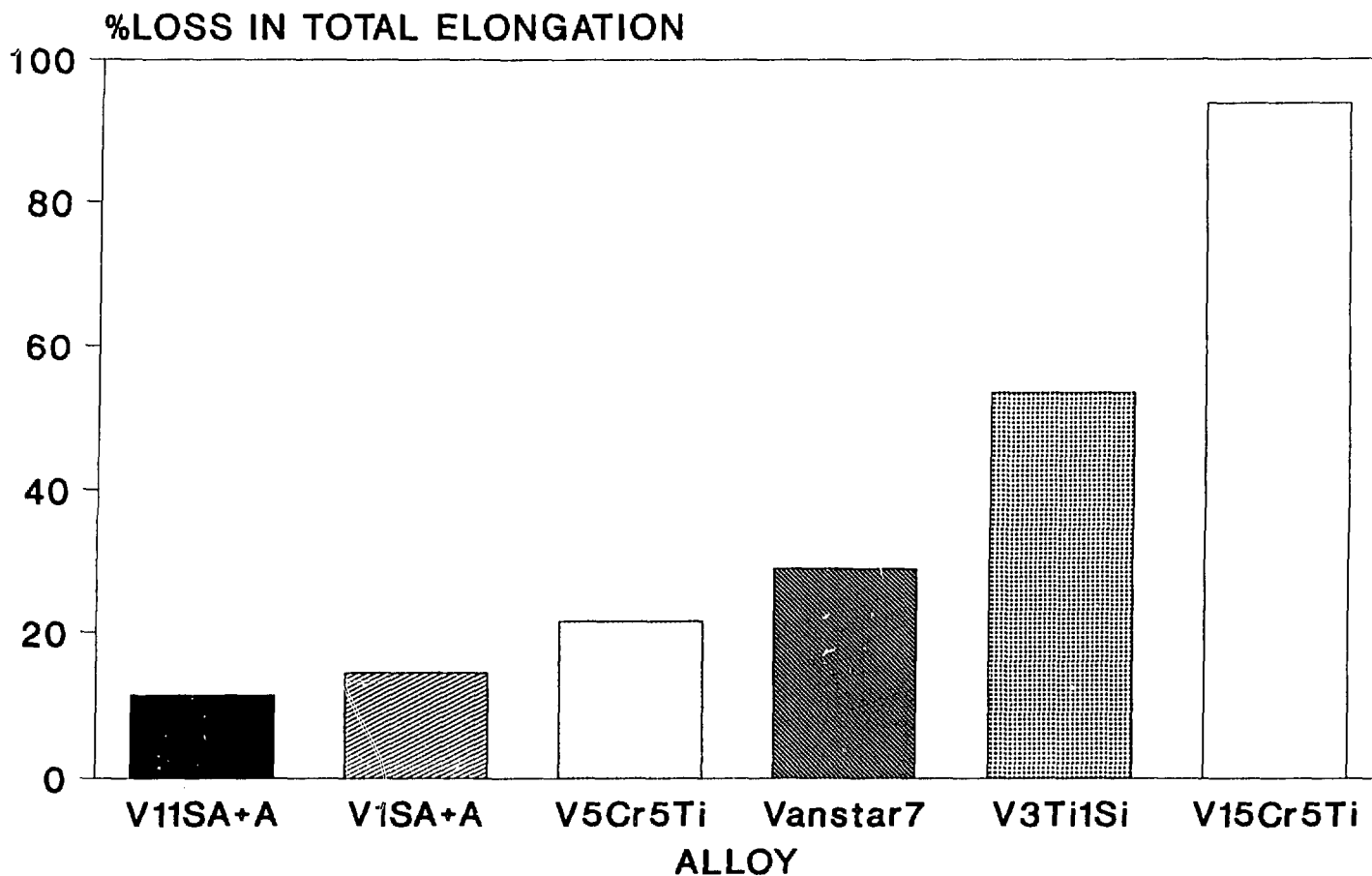

ORNL - B:\EV19

Fig. 9 –

Ductility Changes in V-Ti-Zr-C Alloys Due to 300 appm Implanted Helium

% Change in Total Elong.

Test Temperature, C

—•— V7   —+— V8   —*— V10   —□— V11

ORNL - B:\EV20

Fig. 10 - **Ductility Losses in Vanadium Alloys at 600C Due to 300 appm Implanted Helium**

%LOSS IN TOTAL ELONGATION

ALLOY

B:\EV17

0.1 μm

Fig. 11 – Microstructure of (a) V1-SA+A matrix, (b) V1-SA+A grain boundary, and (c) V1-WW+A matrix after implantation of 300 appm ^{3}He showing how the helium is trapped at Ti-rich MC particles (a, b, and c) and subgrain boundaries (c).
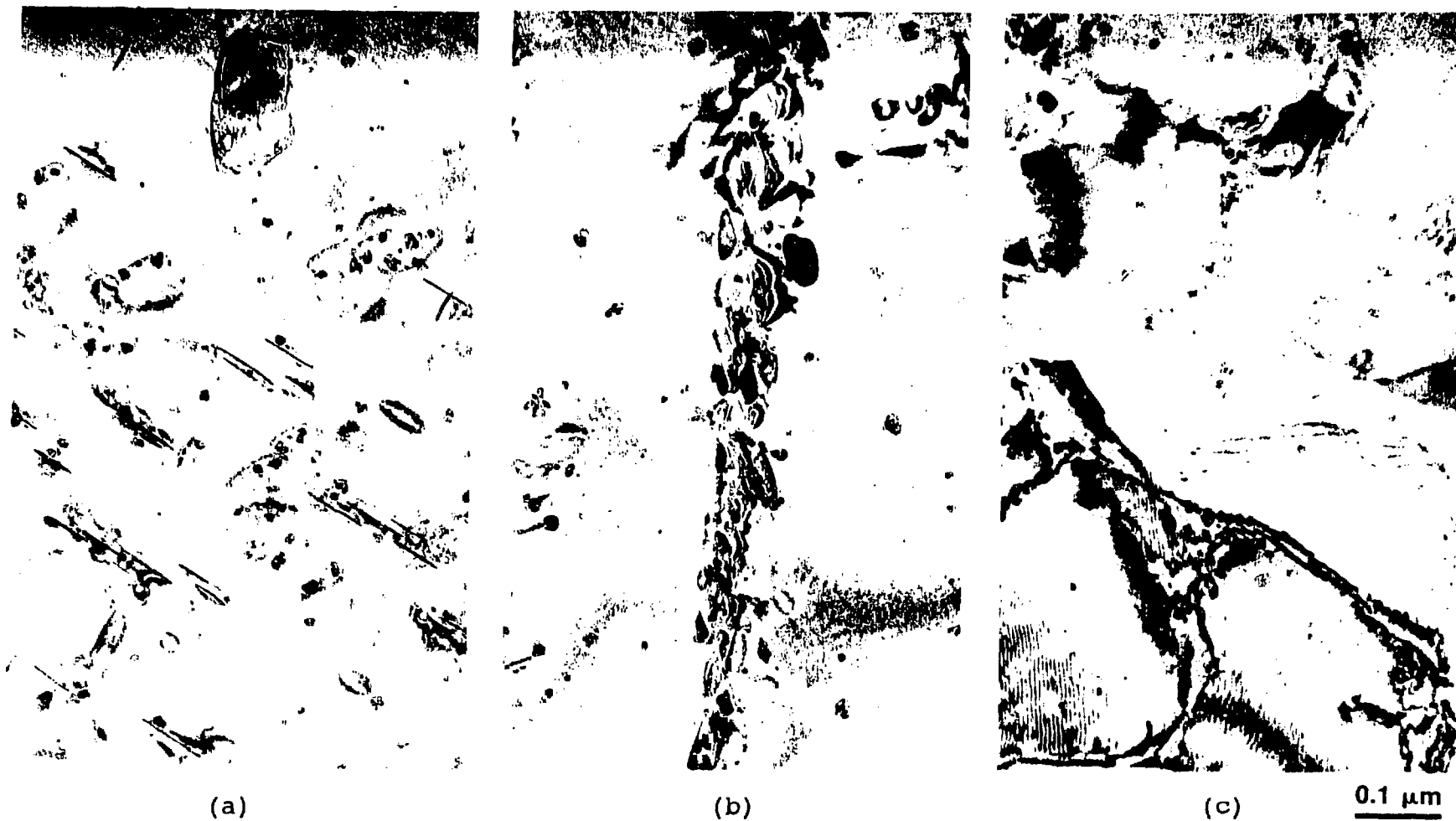
(a)　　　　　　　　　　　　　(b)　　　　　　　　　　　(c)

0.1 μm

Fig. 12 - Microstructure of (a) V11 -SA+A matrix, (b) V11-
SA+A grain boundary, and (c) V11-WW+A matrix
after implantation of 300 appm ^{3}He showing how
the helium is trapped at Ti-rich MC particles
(a, b, and c) and subgrain boundaries (c).